

An In-depth Study of Supported In₂O₃ Catalysts for the Selective Catalytic Reduction of NO_x: The Influence of the Oxide Support

A. Gervasini,[†] J. A. Perdigon-Melon,^{‡,§} C. Guimon,^{||} and A. Auroux^{*,*}

Dipartimento di Chimica Fisica ed Elettrochimica, Università degli Studi di Milano, via Camillo Golgi n. 19, 20133 Milano, Italy, Institut de Recherches sur la Catalyse, CNRS, 2, av. A. Einstein, 69626, Villeurbanne, France, Instituto de Química Física “Rocasolano”, CSIC, c/Serrano 119, 28006 Madrid, Spain, and Laboratoire de Physico-Chimie Moléculaire, 2 avenue du Président Angot, 64053 Pau Cedex 09, France

Received: June 18, 2005; In Final Form: September 26, 2005

The influence of the oxide support (i.e., Al₂O₃, Nb₂O₅, SiO₂, and TiO₂) on the surface properties, reduction and oxidation properties, acid–base properties, and catalytic activity of supported indium oxide catalysts has been investigated by temperature-programmed reduction/oxidation, thermogravimetry coupled to differential scanning calorimetry, ammonia and sulfur dioxide adsorption calorimetry, and reduction of NO_x by ethene in highly oxygen-rich atmosphere. Two series of In₂O₃-containing catalysts at low (≈ 3 wt %) and at theoretical geometric monolayer (from 20 to 40 wt %) In₂O₃ content were prepared and their properties were compared with unsupported In₂O₃ material. Supports able to disperse the In₂O₃ aggregates with high In stabilization gave rise to active catalytic systems. Among the studied oxide supports, Al₂O₃ and, to a lower extent, TiO₂ were found to be the best supports for obtaining active de-NO_x catalysts.

Introduction

The high performance of In-containing catalysts in/on zeolitic and oxide materials has been recently demonstrated for reactions of environmental interest, in particular the selective catalytic reduction of nitrogen oxides by hydrocarbons (HC–SCR process).^{1–9} The main problem with the HC–SCR process remains the identification of a selective catalyst that is able to drive the reduction of NO_x by the hydrocarbon, acting as a reducing species, in a highly oxidizing atmosphere. In fact, on the most active known de-NO_x catalysts, nonselective combustion by oxygen of the hydrocarbon begins to dominate the NO_x reduction above 773 K, and the NO_x conversion concomitantly begins to fall. In addition, the presence of water among the gaseous combustion effluents containing NO_x and vulnerability to deactivation by sulfur oxide prevents zeolite-based materials from being effectively used in this process as viable catalysts.

Among the numerous types of nonzeolitic catalytic systems investigated for NO_x abatement under net oxidizing conditions, In₂O₃^{2–5,10,11} and Ga₂O₃^{12–14} supported on alumina (γ -Al₂O₃) have demonstrated very promising performance. In particular, these metal oxide phases are selective in HC–SCR, being able to predominantly utilize the hydrocarbon for the NO_x reduction while limiting hydrocarbon reactivity with oxygen (combustion). In the first part of this series,¹⁵ a detailed study of a supported In₂O₃ on γ -Al₂O₃ system at different In loading (2 < wt % < 22) has been presented. Surface and bulk properties and catalytic activity toward the selective reduction of NO_x were investigated, paying particular attention to the Brønsted and/or Lewis acidity of the support and metal centers and to the redox character of the metal active species. A balanced presence of In centers and

acidic sites of the alumina support has been found to be involved in de-NO_x reactivity. In this way, it was recognized that not only do the typical properties of supported metal phases affect the catalytic activity (dispersion, distribution, surface structure, etc.), but also the nature of the support dramatically influences the activity and selectivity of the In-supported phase. The poor performances of silica support for numerous transition metal based catalysts toward SCR has been noted.^{6,11} On the other hand, the acidic Brønsted or Lewis oxides (e.g., Al₂O₃, TiO₂, SiO₂–Al₂O₃) are suitable supports for the SCR process.^{16–18} In particular, Maunula et al.⁶ reported on a sol–gel derived alumina on which In₂O₃ and Ga₂O₃, outperform other existing alumina supports.

In this study, we wanted to deepen the understanding of the role of the support on the physicochemical properties and catalytic performances of the In₂O₃-supported phase by studying In-based materials on several different supports. We selected as supports oxides with well differentiated acid properties, both in terms of the nature of their surface sites and their acid strength, including TiO₂, Nb₂O₅, and SiO₂, in addition to Al₂O₃. For each support we also prepared low and high In-loading samples to check the influence of In content. As it is not simple to predict the acid character of a surface when depositing an essentially basic oxide, such as In₂O₃ on an acidic or neutral oxide support, the acidity of the prepared surfaces was carefully studied. The redox properties of the catalysts and the In-dispersion were determined by performing a series of experiments using thermal techniques including temperature programmed reduction and oxidation (TPR–TPO), differential scanning calorimetry (DSC), and thermogravimetric analysis (TGA). To complete the study, the catalytic performances in the selective reduction of NO_x by ethene in an oxygen rich atmosphere were studied and the results interpreted in light of the different surface properties of the catalysts.

* Corresponding author. E-mail: aline.auroux@catalyse.cnrs.fr

[†] Università degli Studi di Milano.

[‡] Institut de Recherches sur la Catalyse.

[§] Instituto de Química Física “Rocasolano”.

^{||} Laboratoire de Physico-Chimie Moléculaire.

Experimental Section

Catalyst Preparation. The samples were prepared by incipient wetness impregnation using the appropriate amounts of In(NO₃)₃·5H₂O from Aldrich (99.9%) in order to obtain two different indium oxide loadings for each support, one series of samples with loadings around 3wt % (hereafter named In(3)/Si (Al, Ti, Nb) or low loading samples) and the second one with an indium oxide loading close to the theoretical geometric monolayer¹⁹ (hereafter named In(hl)/Si (Al, Ti, Nb) or high loading samples). The used supports were γ -Al₂O₃ and SiO₂ from Degussa, TiO₂ DT-51 (anatase) from Rhone-Poulenc, and Nb₂O₅ (obtained by dehydration for 8 h at 523 K in O₂ flow of commercial niobium pentoxide hydrate, niobia HY-340, from Companhia Brasileira de Metalurgia e Mineração Brasil). After impregnation, the samples were dried at 393 K overnight and calcined at 773 K in oxygen flow for 12 h. Bulk In₂O₃ was prepared in the same way, by calcination of indium nitrate at 773 K after drying at 393 K overnight.

Catalyst Characterization. The concentrations of the supported indium oxides were determined by AES–ICP in a Spectroflame-ICP instrument. Surface areas were determined by the BET method from the adsorption of nitrogen at 77 K. The crystallographic structure was examined by X-ray diffraction in a Bruker (Siemens) D5005 apparatus (Cu K α radiation, 0.154 nm). The oxidation states of indium were determined by XPS performed at room temperature with an SSI 301 spectrometer.

The acidity and basicity of the supported indium samples, as well as those of the bare support samples, were determined by adsorption microcalorimetry of NH₃ and SO₂ respectively.²⁰ The samples were pretreated at 673 K in vacuum overnight before the measurements, which were carried out isothermally at 353 K in a heat flow calorimeter (Setaram C80) coupled with a standard volumetric apparatus. Successive doses of gas were sent to the sample until a final pressure of 0.5 Torr was obtained. The sample was then evacuated for 30 min at the same temperature in order to remove the amount physically adsorbed, and a second adsorption was performed. The quantity adsorbed at 0.2 Torr in the first adsorption will be called V_T. The difference between the amounts adsorbed in the first and second adsorptions at 0.2 Torr is the irreversibly chemisorbed amount (V_{irr}).

The redox properties of the supported indium samples have been studied by TPR-TPO experiments. The sample was held on the frit of a U-shape quartz reactor, allowing the reductant or oxidizing gas stream to pass through the sample. In TPR experiments the temperature was increased at 5 K min⁻¹ from room temperature up to 1113 K, under a reducing atmosphere of 5% H₂/Ar (flux 20 cm³ min⁻¹). The temperature was kept at 1113 K for 1 h, followed by cooling under argon atmosphere. After TPR, TPO experiments were carried out using the same experimental conditions, but since volatilization of In₂O₃ takes place at 1123 K,²¹ the temperature was increased only up to 1073 K. The oxidizing atmosphere was 1% O₂/He. The hydrogen or oxygen consumption was determined by means of a TCD (Delsi Instruments DN11). Prior to TPR experiments, the samples were reoxidized under oxygen at 773 K during 3 h and cooled under argon atmosphere.

For the high loading samples, the redox properties have been also studied using a differential scanning calorimeter (DSC) coupled to a microbalance (TGD-DSC 111 from Setaram). This apparatus makes it possible not only to calculate the extent of reduction or oxidation from the weight loss or gain of the sample, but also to simultaneously measure the evolved heat

TABLE 1: Physicochemical Properties of the Samples

sample	S _{ext} m ² g ⁻¹	loading wt % In ₂ O ₃	In/M (molar ratio) (M=Si,Al,Ti)	
			AES–ICP	XPS
In ₂ O ₃	21	100		
SiO ₂	208			
In(3)/Si	215	3.1	0.01	
In(hl)/Si	146	37.2	0.26	0.02
Al ₂ O ₃	112			
In(3)/Al	113	3.2	0.01	0.02
In(hl)/Al	82	26.8	0.13	0.05
TiO ₂	92			
In(3)/Ti	101	3.3	0.02	0.06
In(hl)/Ti	78	20.4	0.15	0.31
Nb ₂ O ₅	108			
In(3)/Nb	88	3.2	0.03	
In(hl)/Nb	71	18.3	0.27	0.39

associated with the process. In contrast to the TPR-TPO experiments, the samples were held in a quartz crucible, which does not allow the reactant gas to pass through the sample. As in TPR-TPO, successive experiments of reduction and oxidation have been carried out. The temperature was increased at 5 K min⁻¹ up to 923 K, keeping this temperature for 30 min, after which the samples were cooled under helium atmosphere. In reduction experiments a total flow of 30 cm³ min⁻¹ with a mixture of 68% hydrogen in helium was used. For oxidation experiments the gas flow was 15 cm³ min⁻¹ and the composition was 46% O₂/He.

de-NO_x Catalytic Activity. The catalytic tests were carried out following the experimental procedure detailed in part I of this series.¹⁵ The experiments were performed at a fixed time of 1.6 g·s·mmol⁻¹ and variable temperature (523–823 K) in a quartz downflow tubular microreactor working close to the atmospheric pressure. The feed mixture was composed of 2500 ppm of NO and 500 ppm of NO₂, 3000 ppm of C₂H₄ and 40,000 ppm of O₂, with He as balance gas. An FTIR spectrometer (Bio-Rad with DTGS detector) was used as an analytical device. NO_x (NO+NO₂) and C₂H₄ conversions as well as CO_x (CO+CO₂) yields were calculated directly from the experimental absorbance values. The N₂ yield was calculated by subtracting the amount of N-containing species flowed out from the reactor from the sum of all the N-containing species fed into the reactor.

Results and Discussion

Physico-Chemical Characterizations. The surface areas of the supports and supported indium oxide samples are summarized in Table 1, as well as the indium oxide loadings determined by AES–ICP. For the low loading samples (\approx 3 wt % In₂O₃), no important variations are observed in the surface area for In(3)/Si, In(3)/Al, and In(3)/Ti samples, except for the In(3)/Nb sample which shows a decrease of 18%. In all cases a marked decrease in surface area takes place for the high loading samples reaching 30, 26, 15 and 34% for In₂O₃ on silica, alumina, titania, and niobia respectively.

The XRD spectra of the high loading samples as synthesized and bulk indium oxide are represented in Figure 1. Alumina, silica, and niobia are amorphous, while titania presents peaks corresponding to anatase. Bulk indium oxide presents a well-crystallized phase. The peak intensities and their 2 θ angles have been identified as characteristic of the cubic structure of In₂O₃ (JCPDS card 6-0416). In the low loading samples, no diffraction lines other than those of the supports are observed (spectra not shown), while in the high loading supported samples diffraction patterns characteristic of well developed crystalline phases of

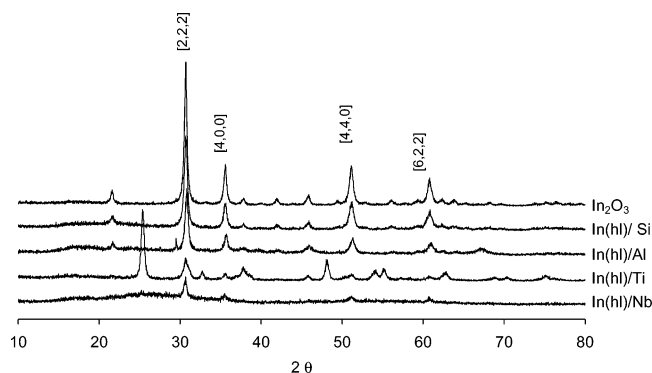


Figure 1. XRD spectra of as-synthesized supported indium oxide samples.

indium oxide are seen. As in the case of bulk indium oxide, these diffraction lines are characteristic of the cubic phase of indium oxide. The intensities of the diffraction peaks and their positions for the different supported indium oxide samples are very similar to bulk indium oxide, indicating that the support does not have a big influence on the crystallization of indium oxide, and in particular does not favor the crystallization in a special plane. The widths at half-height (fwhm) of the diffraction peaks are related to the size of the crystal phases; with respect to this criterion, the crystallinity varies in the order $\text{In}_2\text{O}_3 > \text{In}(\text{hl})/\text{Si} > \text{In}(\text{hl})/\text{Al} > \text{In}(\text{hl})/\text{Nb} > \text{In}(\text{hl})/\text{Ti}$.

XPS gives information on the oxidation state and concentration of indium on the surface of the sample. For all the samples used in the present work, only one oxidation state was found, with In 3d_{5/2} binding energy between 444.5 and 444.8 eV. These values are characteristic of In_2O_3 .²²

The dispersions of the supported phases in the high loading samples can be compared by considering the molar ratios between indium and the metal (M) cation of the support determined by AES–ICP (bulk technique) and by XPS (surface technique). Both values are summarized in Table 1. The sample $\text{In}(\text{hl})/\text{Si}$ presents the lowest surface In/M ratio, despite having the highest indium oxide loading; this is indicative of a poor dispersion of indium oxide phase. $\text{In}(\text{hl})/\text{Nb}$ has a similar In/M ratio determined by AES–ICP, but the In/Nb ratio found by XPS is about 20 times larger, suggesting that most of the indium is located at the surface and that the dispersion is higher. For the $\text{In}(\text{hl})/\text{Ti}$ sample, the In/M ratio determined by AES–ICP is lower than for the $\text{In}(\text{hl})/\text{Nb}$ sample, but the ratio determined by XPS is of the same order in both cases, indicating that the dispersion achieved on titania is bigger than on niobia. The $\text{In}(\text{hl})/\text{Al}$ sample presents an In/M ratio determined by AES–ICP similar to $\text{In}(\text{hl})/\text{Ti}$, but the ratio found by XPS is clearly lower, although better than for the silica sample. This order in the dispersions estimated by XPS ($\text{In}(\text{hl})/\text{Ti} > \text{In}(\text{hl})/\text{Nb} > \text{In}(\text{hl})/\text{Al} > \text{In}(\text{hl})/\text{Si}$) is in good agreement with the crystal sizes found by XRD. This behavior of dispersion can be expected from considerations of surface reactivity: SiO_2 is well-known to have an inert surface, so even if the silica support has the highest surface area of all the supports used, there are comparatively few anchoring sites. Al_2O_3 , TiO_2 , and Nb_2O_5 present more active surfaces (see also below), which allow better dispersions to be obtained.

Acidity and Basicity. The surface acidity and basicity are among the most important features of a solid surface, and influence in a broad range of different reactions. We have studied both properties for bulk indium oxide, the supported indium oxide samples, as well as the bare supports, to determine the influence of the support on the deposited indium oxide.

Figure 2 represents the adsorption heats of ammonia and sulfur dioxide on bulk indium oxide (Figure 2a) and supported indium oxides versus coverage (Figure 2b–e). Table 2 summarizes the total adsorbed amount (V_T) and the irreversible amount (V_{irr}) at 0.2 Torr (see Experimental Section) concerning bulk indium oxide and supported indium oxides. The heats of ammonia adsorption decreased continuously with coverage, while the SO_2 adsorption heat remained constant to an adsorbed amount of $26 \mu\text{mol g}^{-1}$. The fact that the adsorption heats and irreversible volume are clearly higher for SO_2 than for ammonia adsorption indicates that indium oxide can be considered basic rather than acidic.²³

Figure 2b represents the adsorption heats of ammonia and sulfur dioxide on both indium oxide samples supported on silica. The bare support adsorbs neither ammonia nor SO_2 , indicating that the silica surface is mainly inert. The ammonia adsorption heats over both samples drop continuously with coverage. The adsorption of SO_2 gives rise to higher adsorption heats, and for the $\text{In}(\text{hl})/\text{Si}$ sample an initial zone with constant adsorption heats is observed. This feature is also observed for adsorption on bulk indium oxide. Considering that there is no adsorption on SiO_2 , we can conclude that the deposited indium oxide is responsible for the adsorption. Nevertheless, the poor dispersion, due to the inertia of the silica surface, makes the adsorbed quantities very small, even for high indium oxide loading.

The adsorption heats of NH_3 and SO_2 on the $\gamma\text{-Al}_2\text{O}_3$, $\text{In}(3)/\text{Al}$ and $\text{In}(\text{hl})/\text{Al}$ samples are represented in Figure 2c. The heats of ammonia adsorption present an interesting behavior. Except for the initial part (up to $50 \mu\text{mol g}^{-1}$) where the heats of ammonia adsorption on the three samples are identical, the heats of ammonia adsorption on the supported indium oxide samples are lower than on the bare support, with the lowest heats corresponding to the highest amount of indium oxide. The irreversibly adsorbed amounts (see Table 2) decrease in the order $\text{Al}_2\text{O}_3 > \text{In}(3)/\text{Al} > \text{In}(\text{hl})/\text{Al}$. Both results point out that the deposition of indium oxide decreases the acidity of the sample. The heats of SO_2 adsorption on $\gamma\text{-Al}_2\text{O}_3$ and the indium samples supported on alumina present a surprising behavior: while bare alumina and $\text{In}(\text{hl})/\text{Al}$ are identical in the entire range of adsorbed amounts and give rise to very similar irreversibly adsorbed amounts (Table 2), the $\text{In}(3)/\text{Al}$ sample presents lower adsorption heats and a lower irreversibly adsorbed amount. Contrary to expectations, the deposition of indium oxide increases neither the heats nor the adsorption capacity of the bare support.

Adsorption heats of ammonia and SO_2 on TiO_2 and TiO_2 -supported indium samples are represented in Figure 2d. Ammonia adsorption presents the same trend already observed for alumina. The bare support and indium-loaded samples have the same initial adsorption heats (up to $80 \mu\text{mol g}^{-1}$); afterward the adsorption heats are higher on the bare support, and the adsorbed amounts decrease with increasing indium oxide content. The same trend is observed in the irreversibly adsorbed amount (see Table 2), so it can be concluded that the acidity of titania is lowered by indium oxide deposition. Contrary to alumina, the basicity of bare titania is very low, with continuously decreasing heats of SO_2 adsorption. The $\text{In}(\text{hl})/\text{Ti}$ sample presents initial adsorption heats that are markedly higher than for the bare and low indium loading samples. The irreversibly adsorbed amount of SO_2 increases with the amount of supported indium oxide (see V_{irr} in Table 2), indicating that the basicity of titania has been increased by the deposition of indium oxide.

Figure 2e represents the adsorption heats of ammonia and SO_2 on niobia and indium-supported on niobia samples. Except

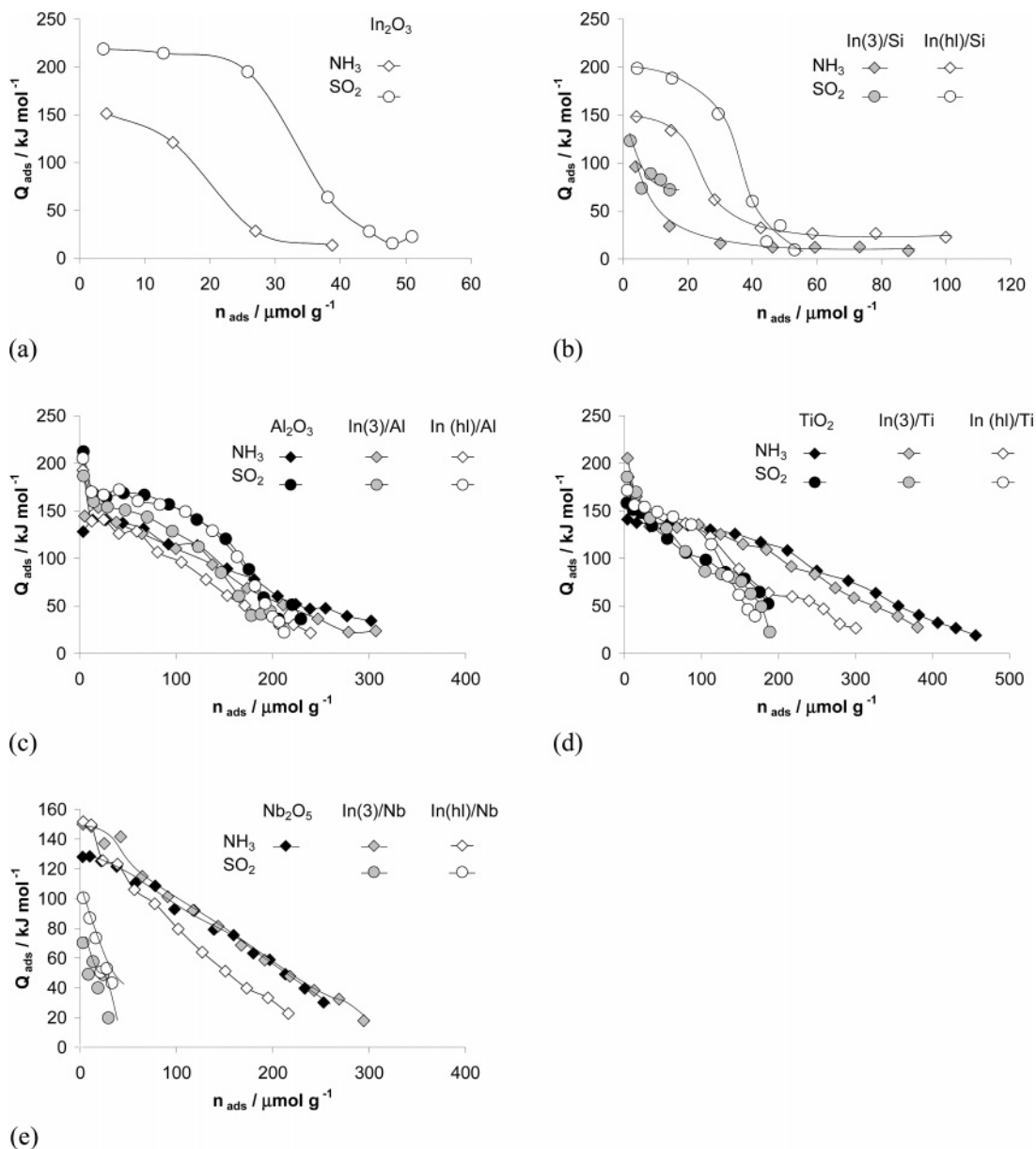


Figure 2. Adsorption heats at 353 K of NH₃ and SO₂ on: (a) indium oxide and indium oxide supported on: (b) silica, (c) γ -Al₂O₃, (d) TiO₂, (e) Nb₂O₅.

TABLE 2: Irreversibly Adsorbed and Total Adsorbed Amounts of NH₃ and SO₂ at 353K under an Equilibrium Pressure of 0.2 Torr

sample	NH ₃		SO ₂	
	V _T μmol g ⁻¹	V _{irr} μmol g ⁻¹	V _T μmol g ⁻¹	V _{irr} μmol g ⁻¹
In ₂ O ₃	66	21	47	40
SiO ₂	58	23	9	5
In(3)/Si	58	23	9	5
In(hl)/Si	77	30	47	40
Al ₂ O ₃	269	161	217	189
In(3)/Al	259	139	192	163
In(hl)/Al	206	125	199	173
TiO ₂	403	265	159	91
In(3)/Ti	348	215	165	102
In(hl)/Ti	270	159	160	128
Nb ₂ O ₅	220	123		
In(3)/Nb	237	130	21	5
In(hl)/Nb	152	84	26	10

in the initial zone where adsorption heats are greater when indium oxide is deposited, the heats of ammonia adsorption are not affected by the presence of indium oxide. The highest

irreversibly adsorbed amount corresponds to the lowest indium loading, following the same trend as for the other supports. The SO₂ adsorption heats and the irreversible amounts increase with the deposited amount of indium oxide. Hence, the deposition of indium oxide decreases the acidity and increases the basicity of niobium oxide.

Redox Properties. The redox properties of the supported indium oxide samples have been studied by means of TPR-TPO experiments. The bare supports also have been tested. The reduction profiles of Al₂O₃ and SiO₂ do not show any hydrogen consumption, while TiO₂ presents a single peak with a maximum at 823 K and a consumption of 0.6 mmol H₂ g⁻¹, and Nb₂O₅ also presents hydrogen consumption at temperatures around 1073 K. Figure 3a represents the TPR profiles of the low loading samples. The In(3)/Si and In(3)/Al samples present broad peaks with onset around 480 K. Table 3 summarizes the total hydrogen consumptions per mol of indium oxide. The complete reduction of indium oxide requires three molecules of hydrogen per molecule of indium oxide. In both cases the reduction is almost 100% of the total deposited amount. In the other two low loading

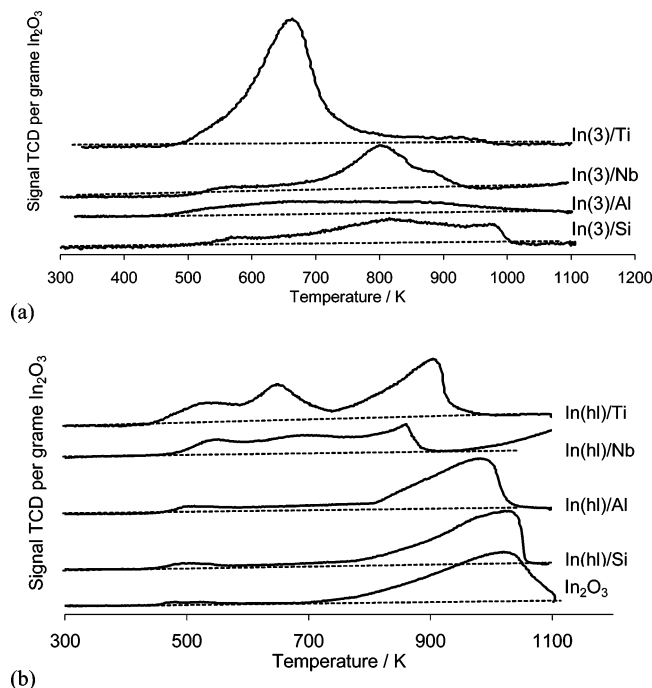


Figure 3. TPR experiments on supported indium oxide samples: (a) low loading, (b) high loading.

TABLE 3: Hydrogen and Oxygen Consumptions in TPR/TPO Experiments on Supported Indium Oxide Samples

sample	TPR (1) mol H ₂ /mol In ₂ O ₃	TPO mol O ₂ /mol In ₂ O ₃	TPR (2) mol H ₂ /mol In ₂ O ₃
In ₂ O ₃	2.8		
In(3)/Si	3.0		
In(hl)/Si	2.7	1.4	
In(3)/Al	3.0		
In(hl)/Al	2.6	0.9	2.9
In(3)/Ti	8.8		
In(hl)/Ti	3.7	1.2	2.5
In(3)/Nb	4.4		
In(hl)/Nb	1.6	--	--

samples the consumed amounts are much larger than the expected ones. For In(3)/Nb, the small difference can be due to reduction of niobia, but in the case of In(3)/Ti the main peak occurs at a lower temperature than titania reduction. This point is discussed below.

The profiles of hydrogen consumption in the TPR experiments for the high loading samples as well as bulk indium oxide are represented in Figure 3b. For bulk indium oxide two peaks are observed, the first one with no well-defined maximum and onset at 448 K, and the second one more intense (96% of the total consumed hydrogen) with an onset at 693 K and maximum at 1028 K. This second peak is almost but not completely developed at the end of the temperature ramp. In this case the total consumption is 2.8 mol of H₂ per mol of In₂O₃, which means that 93% of the indium is reduced. The In(hl)/Si sample presents a profile very similar to bulk indium oxide. The maximum of the second and main peak is at 1030 K, and as in the case of bulk indium oxide, 93% of the supported indium has been reduced. A similar trend is observed for the In(hl)/Al sample, except that after the first peak a constant consumption of hydrogen (not seen in the other samples) is observed up to the beginning of the main peak. The temperature of the maximum of this second and main peak is shifted to a lower temperature (986 K) than for the In₂O₃ and In(hl)/Si samples. On the In(hl)/Ti sample three peaks are detected, with maxima at 543, 650, and 909 K. The positions of the first and third peaks are

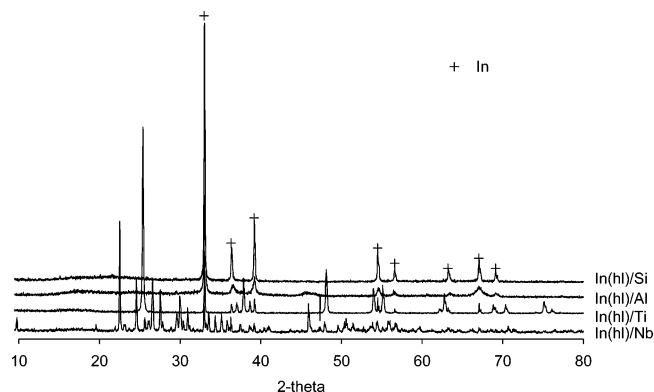


Figure 4. XRD spectra of supported In₂O₃ samples after TPR experiments.

very similar to the peaks found in the other samples. The third peak has been shifted to a lower temperature and its relative intensity is 54%, clearly lower than for the previously mentioned samples where it accounted for about 90% of the total H₂ consumption. The peak with a maximum at 650 K is not observed for the other samples. As remarked above, some titania can be reduced under these conditions, but since the maximum of the reduction peak for the bare support is at 823 K, titania reduction should be masked in the last peak, so it can be supposed that the second peak at 650 K is also due to supported indium oxide. However, a peak at the same temperature was observed for the low loading sample, so another explanation could be that the presence of indium or indium oxide affects the reduction temperature of titania. The amount of hydrogen consumed is higher than expected, probably due to titania reduction. Finally, for the In(hl)/Nb sample we found a profile similar to that of the In(hl)/Ti sample. The two first peaks (548, 701 K) are displaced to slightly higher temperatures, and the last one is cropped when it starts to appear. The last peak, with an onset at 950 K and not totally developed, could be due to niobia reduction. The hydrogen amount consumed (considering only the first three peaks) is clearly lower than the expected one: only 53% of the indium oxide has been reduced.

On the high loading samples, the only indium phase detectable by XRD after TPR is metallic indium (see Figure 4). Since the reduction peaks at low temperature do not appear in the TPR profile of bulk indium oxide, it is difficult to attribute these peaks to different oxidation steps in the reduction from In³⁺ to In⁰. The reduction of bulk indium oxide to metallic indium seems to occur in one step,²⁴ so the behavior observed on the supported samples is generally attributed to the reduction of indium oxide particles of different sizes.² This feature is in agreement with the present results. The dispersion of indium oxide in In(hl)/Si is poor, and due to the high indium content, indium oxide must be forming big aggregates, diminishing the effect of the support and presenting a behavior very similar to bulk oxide. The dispersion of indium oxide in the In(hl)/Al sample is higher, presenting particles of smaller size that are reduced at lower temperature. For In(hl)/Ti this effect is more marked. This sample presents the highest indium oxide dispersion and the highest amount reduced at low temperature. The same behavior is observed for the In(hl)/Nb sample, with two peaks at low temperatures, slightly higher than for the titania-based sample due to the lower dispersion. However, for this sample there are two differences that deserve a more detailed explanation: the reduced amount of indium oxide is only 53%, and the third peak is abruptly cropped at 861 K. It has already been reported that in this sample two effects take place at temperatures around 873 K, namely the crystallization of the

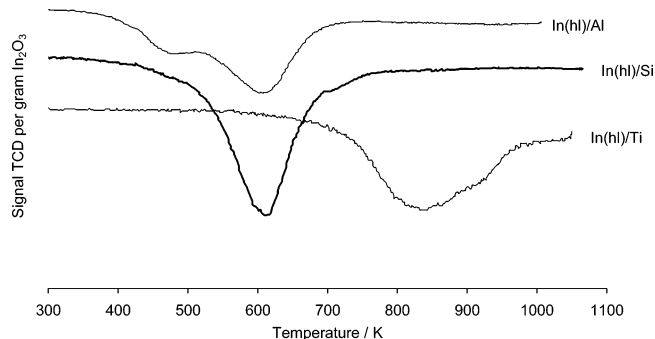


Figure 5. TPO experiments on high loading supported indium oxide samples.

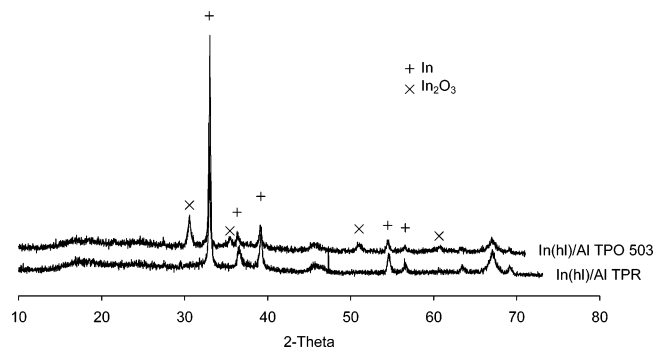


Figure 6. XRD spectra of the In(hl)/Al sample after TPR experiment (In TPR) and after TPO up to 503 K (In_2O_3 TPO 503).

niobia support with an important loss of surface area (which can occlude the indium oxide) and the reaction of the supported indium oxide with niobia to form InNbO_4 .²⁵ Both processes are detected in the XRD spectra measured after the TPR experiments (Figure 4), where well crystallized niobium oxide in hexagonal phase and InNbO_4 are both detected, explaining the sharp decrease in the amount of indium oxide available to be reduced.

The TPO experiments carried out after TPR evidenced remarkable differences among the different samples (Figure 5). For bulk indium, no consumption of oxygen was detected. On In(hl)/Si, only one peak is observed, with a maximum at 612 K, and the amount of oxygen consumed is very close to the expected amount (1.5 mol oxygen per mol of generated indium oxide). The In/Al sample presents two different peaks. The oxidation begins at lower temperatures than for In(hl)/Si, but the second and more important peak has its maximum at the same temperature as for the In(hl)/Si sample. The XRD spectrum obtained on a sample where TPO was stopped at 503 K (Figure 6) shows the peaks corresponding to indium oxide and metallic indium, suggesting that, as in the case of reduction, the oxidation peak at low temperature is probably due to the smallest indium crystallites and not to intermediate oxidized species. The In(hl)/Ti sample presents only one peak, larger and with an onset and a maximum at higher temperatures than the two other samples. This difference can hardly be attributed to differences in the size of indium particles, because according to XRD, the particle sizes must be similar; so in some way titania stabilizes metallic indium. The oxidation process is more affected by the support than the reduction, where the main differences are related to particle size. The temperature of the maximum in TPO experiments is lower than in TPR experiments, even if after TPR experiments indium particles have been synthesized.

For In(hl)/Al and In(hl)/Ti, a second TPR experiment was carried out after TPO; the profile of this second TPR is represented in Figure 7. Comparing this profile with the TPR carried out on the fresh sample (Figure 3b), a huge change is

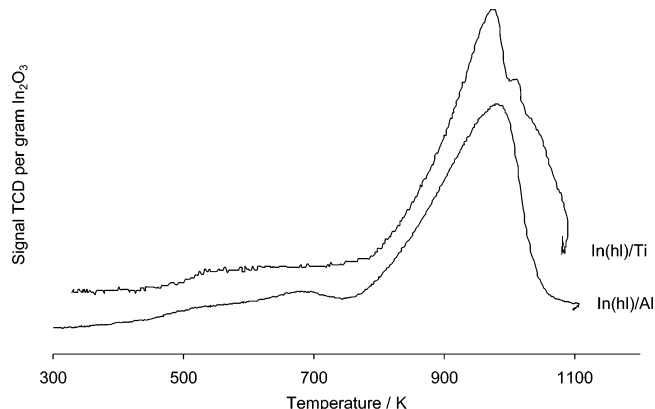


Figure 7. Second TPR experiments after first TPR-TPO cycle for samples In(hl)/Ti and In(hl)/Al.

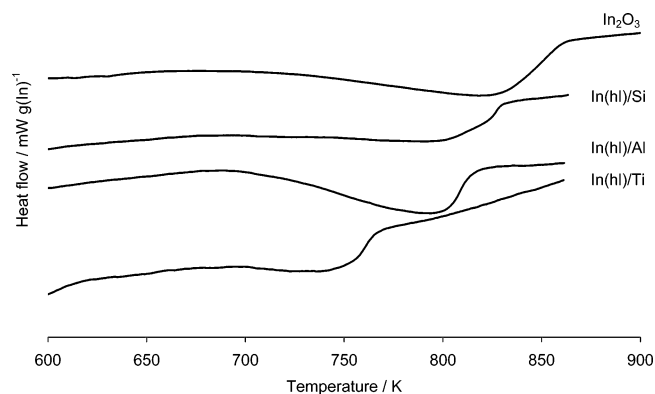


Figure 8. Heat flow profiles of reduction of In_2O_3 and supported indium oxide samples.

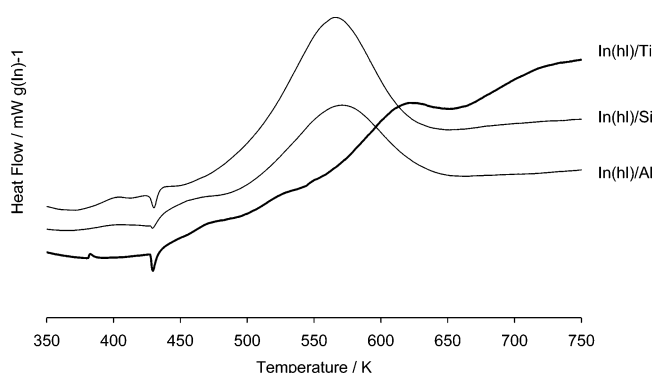
observed, especially for the In(hl)/Ti sample. The reduction peak that took place at low temperature in the first TPR run has disappeared in the second run, where reduction occurs only at high temperature. For the In(hl)/Ti sample the reduction peak temperature changes from 910 to 979 K, with a profile quite similar to the TPR of bulk indium or In/Si. The XRD pattern after the TPR experiments (Figure 4) shows very narrow peaks, typical of metallic indium, indicating that after reduction at high-temperature crystalline indium has been formed, as the behavior of the supported indium oxide becomes closer to bulk indium oxide. At the end of these experiments, a decrease in surface area was observed, confirming the loss of dispersion. As in the TPR on the fresh sample, the consumption of hydrogen is very close to the expected 3 mol of H_2 per mol of In_2O_3 , indicating that the process of reduction/oxidation of indium oxide is reversible.

In addition to TPR-TPO, experiments of oxidation and reduction have been carried out on the high loading samples by TG-DSC. The heat flow profiles for reduction experiments are presented for all samples in Figure 8. Though these results could not be compared quantitatively with TPR experiments because of the different experimental conditions (reactant mixture composition, reactant gas flow, etc.), the results are qualitatively the same. As in TPR, In(hl)/Ti is the most easily reduced sample, followed by In(hl)/Al, In(hl)/Si, and bulk indium oxide. In all cases the extent of reduction estimated from the mass loss (0.17 g per gram of In_2O_3 reduced) is very close to the expected extent of reduction (see Table 4), suggesting that the total reduction of indium oxide takes place. In some cases the mass loss is larger than expected, probably due to water loss. Even if the main loss of water occurs up to 413 K, the most strongly adsorbed water could be retained up to 700

TABLE 4: Mass Variation and Evolved Heat in the Reduction/Oxidation Process of Supported Indium Oxide Samples

sample	reduction		oxidation	
	mass ^a %	heat kJ (mol In ₂ O ₃) ⁻¹	mass ^a %	heat kJ (mol In) ⁻¹
In ₂ O ₃	109	171.4		
In(hl)/Si	107	95.6	110	-284.9
In(hl)/Al	107	108.9	102	-204.8
In(hl)/Ti	91	64.9	94	-39.5

^a Ratio between the experimental mass loss/gain during reduction/oxidation and the corresponding to theoretical mass variation (%).

**Figure 9.** Heat flow profiles of oxidation of supported indium samples.

K. The measured heats are in the order In₂O₃ > In(hl)/Al > In(hl)/Si > In(hl)/Ti. It is useful to remember that the measured heat includes not only the reduction heat but also the melting of metallic indium. The melting point of metallic indium is 426.6 K,²¹ which is lower than the reduction onset in all cases, so reduction and fusion must take place at the same time. This fact is well observed in bulk indium oxide, for which the cooling ramp features a very narrow exothermic peak without associated mass variation and centered at 427.2 K, indicating the solidification of metallic indium. For the other samples this peak does not occur (Figures not shown).

No oxidation is observed in the case of reduced bulk indium. For the three other samples the oxidation gives rise to an exothermic peak (Figure 9). The same behavior is observed as in the TPO experiments: In(hl)/Al presents two oxidation peaks and the lowest onset temperature of the three samples, while In(hl)/Si and In(hl)/Ti present only one oxidation peak, at a higher temperature for In(hl)/Ti. Contrary to reduction experiments, the melting point of indium is seen for all three samples, always at the same temperature (430.9 K), indicating the absence of influence of the support on the melting point, probably due to the sintering of metallic indium particles. It is interesting to point out that in the case of In(hl)/Al reoxidation takes place before and during the fusion of metallic indium, while for In/Si and especially In/Ti the metallic indium melts before oxidation.

The measured heats in the reduction process follow the order In₂O₃ ≫ In(hl)/Al ≅ In(hl)/Si > In(hl)/Ti, while in the oxidation process the order found is In(hl)/Si > In(hl)/Al ≫ In(hl)/Ti. It is interesting to note that the measured oxidation heat for the In(hl)/Ti sample is much lower than for the two other samples, even though the weight increase is very similar to that expected for the total oxidation. This fact and the higher oxidation temperature suggest that the oxidation of metallic indium on this sample occurs in a different manner from the two other samples.

de-NO_x Catalytic Activity. The activity of the indium-containing catalysts in the reduction of NO_x by C₂H₄ in high

oxygen content atmosphere is dramatically dependent on the support. Figures 10 and 11 show the results obtained for the reaction performed in the 473–773 K temperature range on the In₂O₃ phases dispersed over alumina, titania, niobia, and silica supports. The results for the unsupported In₂O₃ bulk oxide are also presented in Figures 10 and 11 for comparison.

For each catalytic system, both the NO and NO₂ conversions (Figure 10a–e) and the C₂H₄ conversions to CO and CO₂ (Figure 11a–e) are shown. As a general trend, the reactivity of NO₂ is higher than that of NO. The values of the NO₂ conversion attained 70% over In₂O₃ supported on alumina, about 40–50% over In₂O₃ supported on titania or silica, and about 30–40% over bulk In₂O and In₂O₃ supported on niobia. The curves of NO₂ conversion as a function of temperature display a typical trend. At low temperatures (below 573 K), there is a rapid increase of NO₂ conversion with temperature. As it is not possible to observe a parallel high ethene conversion, the very high NO₂ consumptions observed could be ascribed to nitrite and/or nitrate formation on the catalyst surfaces. The observed behavior is in agreement with some recent literature findings.²⁶ For higher temperatures, two different behaviors of the NO₂ conversion-temperature curves could be observed. The In₂O₃ phases on alumina, titania, and silica display a more or less regular increasing trend of NO₂ conversion with temperature, attaining a maximum value in the cases of In/Al and In/Ti but not in the case of In/Si. This second increase in NO₂ conversion with temperature could be associated with NO₂ reduction to N₂, as in parallel a high C₂H₄ conversion to CO₂ was observed (Figure 11a–e). Meanwhile, on the niobia-supported system, no increasing trend of NO₂ conversion could be observed in the entire temperature range investigated.

The curves of NO conversion vs temperature follow a different trend from those of NO₂ conversion, in particular in the low-temperature range (below 573 K) where no increase of the NO conversion could be observed. In the 573–823 K temperature interval, a noticeable increase in the NO conversion was observed for the catalysts on the alumina, titania, and silica supports, but not on the niobia support, in agreement with the behavior of the NO₂ conversions. In this case too, the NO conversion could be associated with N₂ formation due to the high C₂H₄ consumption observed.

C₂H₄ was selectively oxidized by NO and NO₂ to CO₂. Only very limited amounts of CO were detected over the various catalytic systems (Figure 11a–e). The CO yields decreased even further at temperatures higher than 773 K. The highest amounts of CO formation were observed over In₂O₃ supported on niobia and silica. On these systems the CO₂/CO ratio in the 773–823 K interval was around 5–20, while on the more active catalysts (with alumina and titania supports) the CO₂/CO ratio was as high as 15–40. In any case, quantitative C₂H₄ conversion to CO₂ was never observed. The highest CO₂ yields were observed over In/Al, In/Ti, and In/Si (about 70%). In/Nb was poorly active, both for reducing NO_x and for oxidizing C₂H₄. Bulk In₂O₃ had a marked oxidizing character, as demonstrated by the high amount of CO₂ formed.

The most selective catalysts were the In/Al and In/Ti systems. They could be distinguished from the others by a higher ratio between the amount of NO_x reduction to N₂ and the amount of C₂H₄ oxidation to CO₂ (compare Figures 10 and 11). This so-called *reaction selectivity* is due to the coexistence of two main parallel reactions in the HC–SCR process.^{27–28} The two oxidant species O₂ and NO_x are present simultaneously in the feed mixture, and they compete for the oxidation of ethene. Because the amount of O₂ is much higher than that of NO_x in the feed,

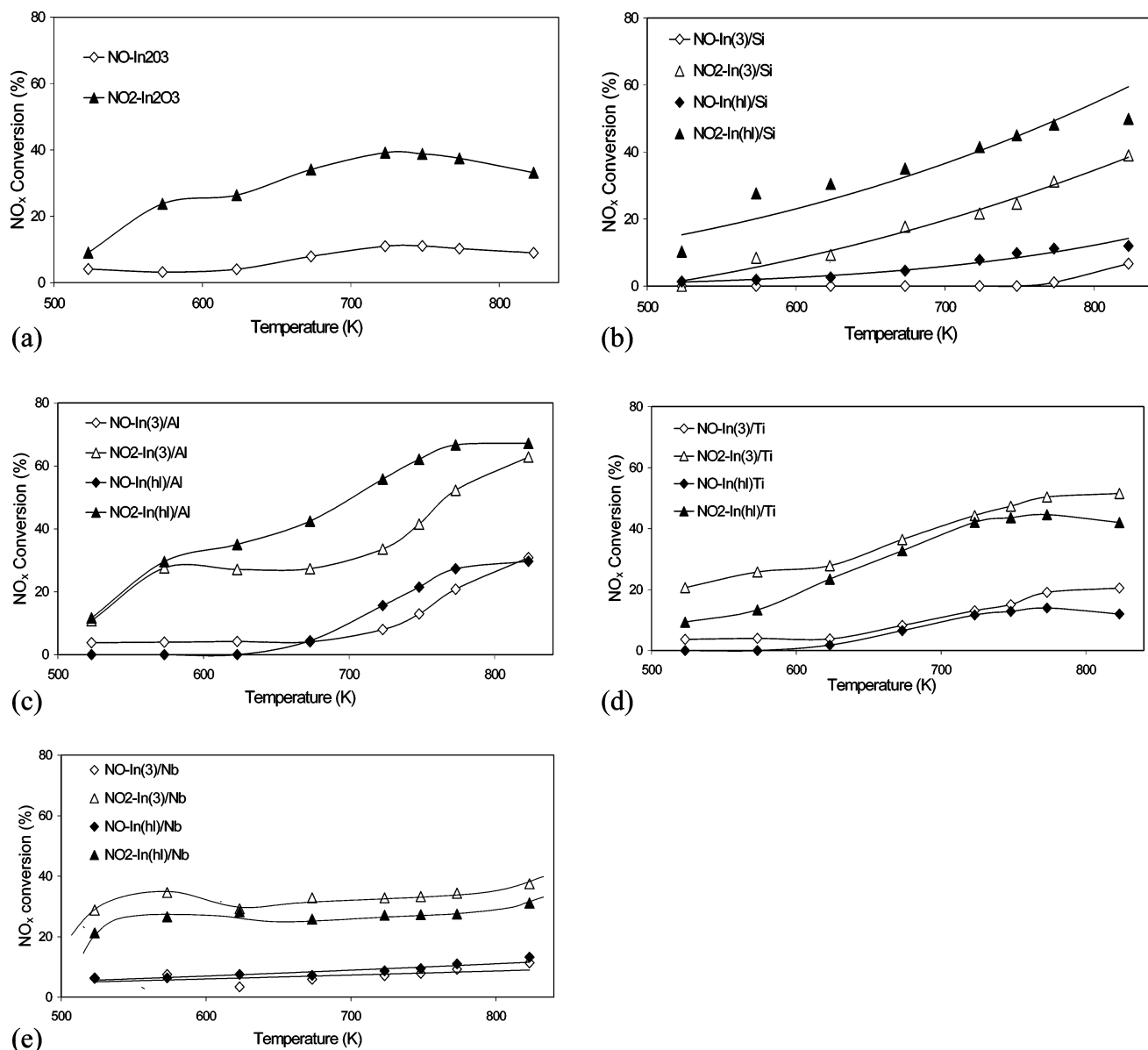


Figure 10. Conversion of NO_x as function of reaction temperature for (a) bulk indium oxide and the high (filled symbols) and low (open symbols) loading indium oxide catalysts supported on: (b) silica, (c) alumina, (d) titania, (e) niobia.

the combustion of the hydrocarbon naturally occurs with a higher rate than the parallel reaction between C_2H_4 and NO_x . Selective catalytic systems are able to favor the involvement of the hydrocarbon in the NO_x reduction reaction, limiting the hydrocarbon combustion. Unlike the supported catalysts, bulk In_2O_3 showed very poor selectivity.

It is interesting to observe the influence of the In loading on the activity and selectivity of the catalysts for the different supports. As regards C_2H_4 combustion, all the catalytic systems followed a general trend: the high In loading systems were much more active than those with low In loadings. However, no general common behavior could be observed for the NO_x conversion. The high loading In_2O_3 catalysts supported on alumina and silica, $\text{In}(\text{hl})/\text{Al}$ and $\text{In}(\text{hl})/\text{Si}$, had a higher activity for NO_x reduction than the corresponding low In_2O_3 loading systems. The In_2O_3 systems supported on titania and niobia had an opposite behavior. The observed behavior is difficult to explain; it could be related to differences in the In_2O_3 dispersion on the surface of the different supports. Small amounts of very poorly dispersed In_2O_3 gave rise to a low activity, as evidenced by the niobia- and silica-supported systems. On the contrary,

when In_2O_3 was well dispersed on the surface of the support, high activity could be observed, as in the case of alumina and titania.

Figure 12 gives a comparative view of the collected results, in terms of N_2 yield over the various studied catalysts. The better activity of the alumina and titania supports clearly emerges. No remarkable differences could be detected between the bulk In_2O_3 and the In_2O_3 systems supported on niobia and silica. It can be inferred that on these supports In_2O_3 has not been well dispersed; this can be due to the surface properties of these oxides. Silica is very poorly acidic and niobia is an acidic oxide possessing poor amphoteric properties. The balanced presence of basic and acidic sites on the support surfaces could play a key role in stabilizing the dispersed In_2O_3 particles, limiting their aggregation into large indium *islands*, which are not as active in reducing NO_x .

Because of the incomplete coverage of the supports, both the metal oxide and support sites might participate to the complex reaction mechanism of selective reduction of NO_x . Following the reaction mechanism recently proposed for $\text{Ga}_2\text{O}_3/\text{Al}_2\text{O}_3$ and $\text{In}_2\text{O}_3/\text{Al}_2\text{O}_3$ systems by Haneda et al.,³ the surface species of

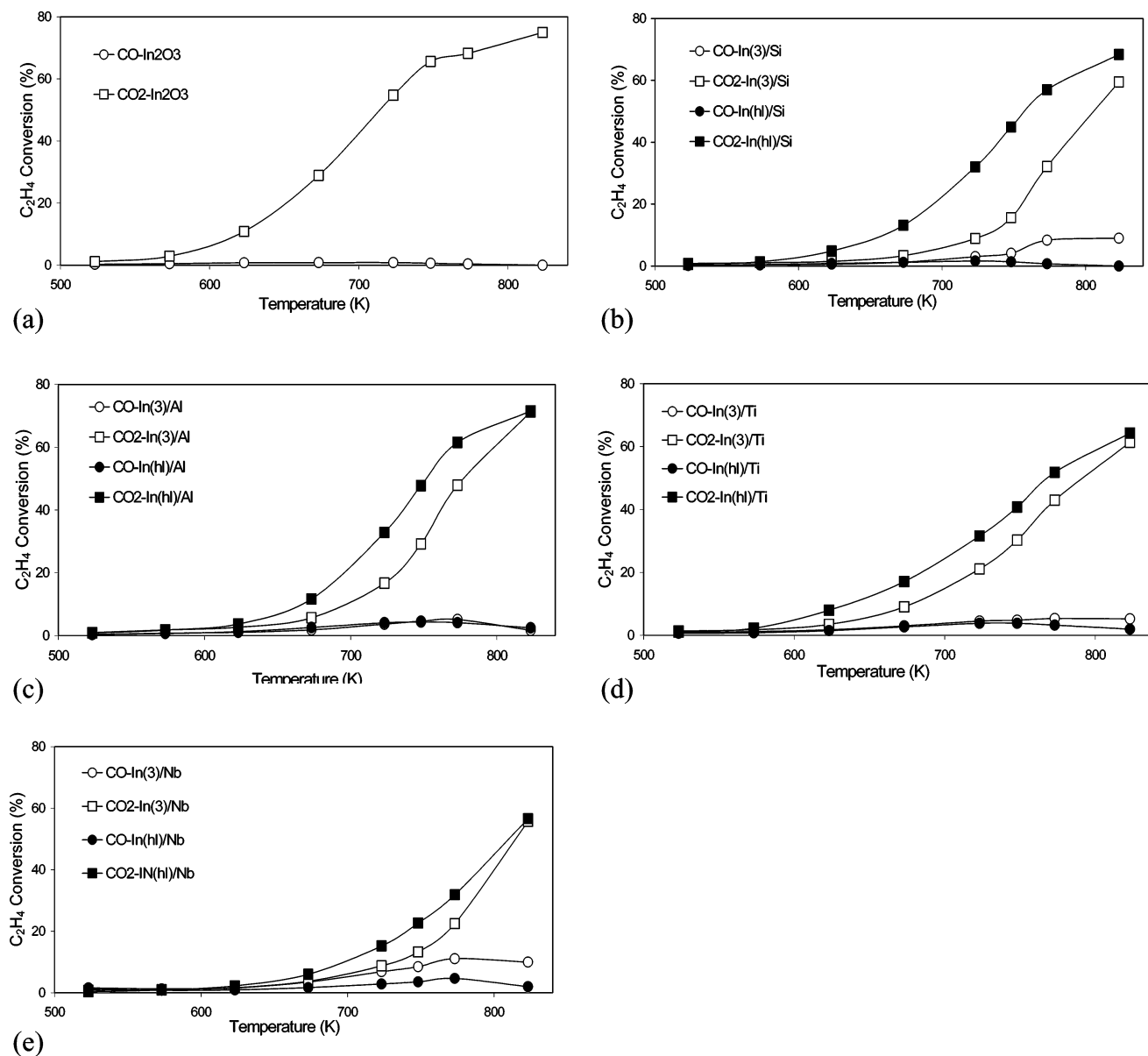


Figure 11. Conversion of C_2H_4 to CO_x as function of reaction temperature for (a) bulk indium oxide and the high (filled symbols) and low (open symbols) loading indium oxide catalysts supported on: (b) silica, (c) alumina, (d) titania, (e) niobia.

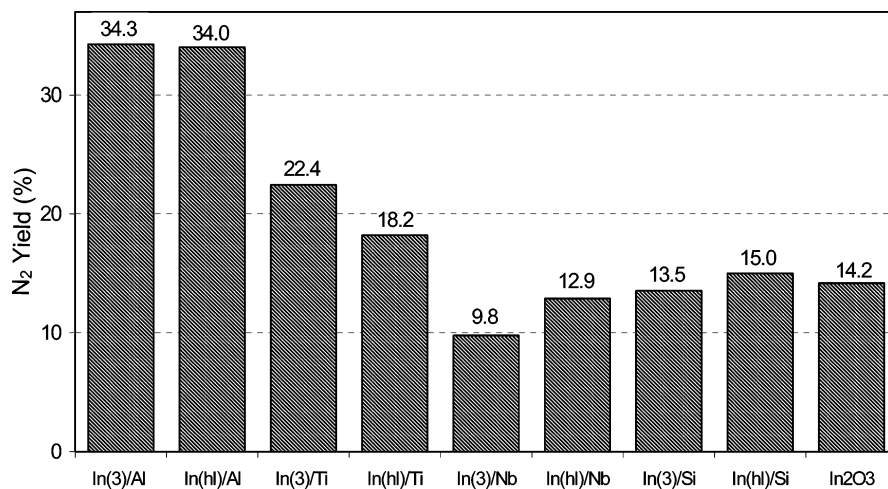


Figure 12. Comparison of N_2 yields obtained for the low and high In loading catalysts over the different supports and bulk indium oxide at 823 K.

the support can be primarily involved in nitrate formation, which can explain the low NO_2 (and NO) conversion on silica and

niobia supports. The surface nitrate species can react with the hydrocarbon, leading to thermally unstable organic nitro and

nitrile compounds that can be oxidized by O₂ or reduced by NO_x, leading to the final N₂ product. On the other hand, nitrate species formed on dispersed In₂O₃ species can act as strong oxidant for the hydrocarbon, realizing a direct red-ox reaction justifying that the poorly dispersed In₂O₃ particles are less active than the highly dispersed ones.

Conclusions

The selective reduction of NO_x by hydrocarbons (HC-SCR) was studied over four different catalytic systems prepared by dispersing various amounts of In₂O₃ over different supports. Indium oxide can be considered as a basic solid. As a general rule, the global acidity was decreased and the basicity increased upon deposition of indium oxide on the support.

Indium oxide is reversibly reduced and oxidized; the temperature of reduction is mostly related to the particle size, whereas oxidation is more influenced by the support. The oxidation of indium oxide takes place at a lower temperature than the reduction. The In(hl)/Ti sample presents the highest oxidation temperature, indicating that titania stabilizes metallic indium.

Alumina and titania were found to be the best supports in order to prepare active and selective de-NO_x catalysts. The better stabilization of In₂O₃ by titania, detected by XRD and TPR/TPO profiles, could explain the higher activity in the reaction of NO_x reduction by hydrocarbons observed for the low loading sample In(3)/Ti. More generally, supports that are able to disperse the In₂O₃ aggregates with high In stabilization could give rise to active catalytic systems.

References and Notes

- (1) Berndt, H.; Schütze, F.-W.; Richter, M.; Sowade, T.; Grünert, W. *Appl. Catal. B* **2003**, *40*, 51.
- (2) Park, P. W.; Ragle, C. S.; Boyer, C. L.; Balmer, M. L.; Engelhard, M.; McCready, D. *J. Catal.* **2002**, *210*, 97.
- (3) Haneda, M.; Joubert, E.; Ménézo, J. C.; Duprez, D.; Barbier, J.; Bion, N.; Daturi, M.; Saussey, J.; Lavalley, J. C.; Hamada, H. *J. Mol. Catal. A* **2001**, *175*, 179.
- (4) Sulikowski, B.; Kubacka, A.; Wloch, E.; Schay, Z.; Cortés Corberán, V.; Valenzuela, R. X. *Stud. Surf. Sci. Catal.* **2000**, *130*, 1889.
- (5) Serban, M.; Halasz, I.; Datta, R. *Catal. Lett.* **1999**, *63*, 217.
- (6) Maunula, T.; Kintaichi, Y.; Inaba, M.; Haneda, M.; Sato, K.; Hamada, H. *Appl. Catal. B* **1998**, *15*, 291.
- (7) Requejo, F. G.; Ramallo-López, J. M.; Ledo, E. J.; Miró, E. E.; Pierella, L. B.; Annunziata, O. A. *Catal. Today* **1999**, *54*, 553.
- (8) Schmidt, C.; Sowade, T.; Schütze, F.-W.; Richter, M.; Berndt, H.; Grünert, W. *Stud. Surf. Sci. Catal.* **2001**, *135*, 4973.
- (9) Schütze, F.-W.; Berndt, H.; Richter, M.; Lucke, B.; Schmidt, C.; Sowade, T.; Grünert, W. *Stud. Surf. Sci. Catal.* **2001**, *135*, 1517.
- (10) Miyadera, T.; Yoshida, K. *Chem. Lett.* **1993**, 1483.
- (11) Hamada, H.; Kintaichi, Y.; Sasaki, M.; Ito, T.; Tabata, M. *Appl. Catal.* **1991**, *75*, L1.
- (12) Tabata, T.; Hamada, H.; Suganuma, F.; Yoshinari, T.; Tsuchida, H.; Kintaichi, Y.; Sasaki, M.; Ito, T. *Catal. Lett.* **1994**, *25*, 55.
- (13) Hamada, H.; Kintaichi, Y.; Yoshinari, T.; Tabata, M.; Sasaki, M.; Ito, T. *Catal. Today* **1993**, *17*, 112.
- (14) Subramanian, S.; Kudla, R. J.; Chun, W.; Chattha, M. S. *Ind. Eng. Chem. Res.* **1993**, *32*, 1805.
- (15) Perdigon-Melon, J. A.; Gervasini, A.; Auroux, A. *J. Catal.* **2005**, *234*, 421.
- (16) Haneda, M.; Kintaichi, Y.; Inaba, M.; Hamada, H. *Appl. Surf. Sci.* **1997**, *121/122*, 391.
- (17) Kintaichi, Y.; Haneda, M.; Inaba, M.; Hamada, H. *Catal. Lett.* **1997**, *48*, 121.
- (18) Ren, L.; Zhang, T.; Tang, J.; Zhao, J.; Li, N.; Lin, L. *Appl. Catal. B* **2003**, *41*, 129.
- (19) Innes, W. B. In *Catalysis*, Vol. I, Fundamental principles (Part I); Emmett, P. H. Ed.; Reinhold Publishing Corporation: New York, 1954; Chapter 6, p 258.
- (20) Auroux, A. *Top. Catal.* **1997**, *4*, 71. Auroux, A. *Top. Catal.* **2002**, *19*, 205.
- (21) *Handbook of Chemistry and Physics*, 70th ed; Weast, R. C.; Lide, D. R.; Astle, M. J.; Beyer W. H., Eds.; CRC Press: Boca Raton, 1989–1990.
- (22) Poznyak, S. K.; Golubev, A. N.; Kulak, A. I. *Surf. Sci.* **2000**, *545–456*, 396.
- (23) Choudhary, V. R.; Jana, S. K.; Kiran, B. P. *J. Catal.* **2000**, *192*, 257.
- (24) Mihályi, R. M.; Beyer, H. K.; Mavrodinova, V.; Minchev, Ch.; Neinska, Y. *Micropor. Mesopor. Mater.* **1998**, *24*, 143.
- (25) Petre, A. L.; Perdígón-Melón, J. A.; Gervasini, A.; Auroux, A. *Catal. Today* **2003**, *78*, 377.
- (26) Haneda, M.; Kintaichi, Y.; Bion, N.; Hamada, H. *Appl. Catal. B* **2003**, *42*, 57.
- (27) Gervasini, A.; Carniti, P.; Ragaini, V. *Appl. Catal. B* **1999**, *22*, 201.
- (28) Carniti, P.; Gervasini, A.; Modica, V. H.; Ravasio, N. *Appl. Catal. B* **2000**, *28*, 175.